ACS OMEGA

Open Access

http://pubs.acs.org/journal/acsodf

Article

Unlocking the Potential of Magnetic Refrigeration: Investigating the Compatibility of the Ga-Based Liquid Metal with a La(Fe,Mn,Si)$_{13}$H$_z$ Magnetocaloric Material for Enhanced Long-Term Stability

Keerthivasan Rajamani,* Muhammet Sadaka Toprak, Fengqi Zhang, Achim Iulian Dugulan, Ekkes Brück, Theo van der Meer, and Mina Shahi

Cite This: *ACS Omega* 2023, 8, 49027−49036

Read Online

ACCESS | Metrics & More | Article Recommendations

ABSTRACT: Magnetic refrigeration (MR) is a cutting-edge technology that promises high energy efficiency and eco-friendliness, making it an exciting alternative to traditional refrigeration systems. However, the main challenge to its widespread adoption is cost competitiveness. In this context, the use of liquid metals as heat transfer liquids in the MR has been proposed as a game-changing solution. Unfortunately, the toxicity and flammability of these liquid metals have raised serious concerns, limiting their practical use. In this study, we investigate the compatibility of a nontoxic and nonflammable GaInSn-based liquid metal with a magnetocaloric material, La(Fe,Mn,Si)$_{13}$H$_z$, over a 1.5 year period. Our findings reveal nearly a 14% reduction in specific cooling energy and peak-specific isothermal magnetic entropy change for the considered magnetocaloric material. Our study provides valuable insights into the long-term stability of magnetocaloric materials and their compatibility with liquid metals, facilitating the development of more cost-effective and sustainable MR systems.

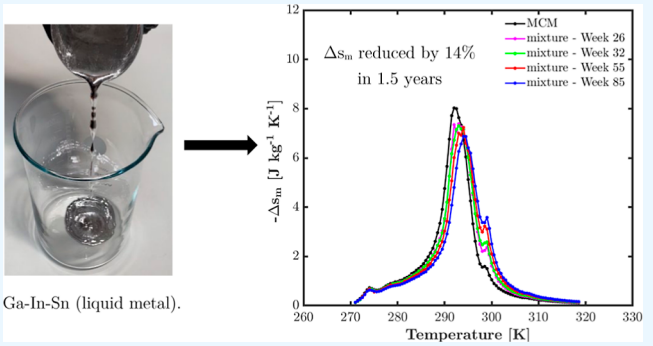

1. INTRODUCTION

Refrigeration accounts for a significant share of global electricity consumption,[1,2] and traditional vapor compression refrigeration systems have been the dominant technology for a long time. However, emerging research in the field of magnetic refrigeration (MR) is opening new doors for energy-efficient and environmentally friendly refrigeration solutions. Studies have shown that MR systems based on the magnetocaloric effect can be up to 10 to 20% more energy-efficient than traditional compressor-based systems.[3] This is a significant improvement with a positive impact on our environment.[4]

One of the key factors in the success of MR is the frequency of the thermodynamic cycle, which plays an essential role in economic competitiveness against traditional vapor compression refrigeration systems. While the specific cooling energy per cycle of MR is lower than that of traditional systems, this can be compensated by operating the system at a higher frequency, typically 1 to 2 orders of magnitude higher.[5] Moreover, the materials used in MR are relatively environmentally friendly, making this technology a promising solution for reducing greenhouse gas emissions and promoting sustainable development.[4] However, the cost of MR systems has been a significant obstacle to their widespread adoption. Research has shown that the magnetocaloric material and magnet assembly account for nearly two-thirds of the total cost of a magnetic refrigerator.[6] Therefore, the cost per unit of cooling power is a crucial parameter in determining the economic competitiveness of MR systems.

In a comparative analysis between a 50 W compressor for a traditional vapor compression system and a magnetocaloric material and magnet assembly for a magnetic refrigerator, it was found that the operating frequency of MR systems should be at least 2 to 5 Hz (depending on the costs of components) to match the costs of an equivalent compressor.[6] Similarly, a study on magnetic heat pumps (the reverse of a refrigerator) found that an operational frequency of around 10 Hz is required for magnetic heat pumps to have comparable manufacturing costs to vapor compression heat pumps.[6,7]

The above discussion on the operating frequency focused on the magnetocaloric material and the magnet arrangement; however, the heat transfer liquid used in the system also plays a crucial role in its performance and cost. While water, alcohol,

Received: September 5, 2023
Revised: November 14, 2023
Accepted: November 16, 2023
Published: December 12, 2023

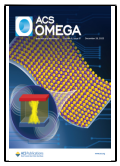

and water−alcohol mixtures with corrosion inhibitors are commonly used, liquid metals such as mercury, sodium−potassium (NaK), and GaInSn alloy offer superior thermal properties and performance.[16] Among these, GaInSn alloy (for example, GaInSn—68.5, 21.5, 10 wt %, known by its trade name Galinstan) is particularly attractive due to its nontoxicity and safety at room temperature, as well as its high thermal conductivity and low specific heat.[8,9] These properties enable a reduced size of the system components and lower manufacturing costs.

GaInSn is a nontoxic liquid metal at room temperature that forms an oxide layer when exposed to air.[9−11] Its thermal conductivity is 27 times more than that of water,[12] allowing for faster heat transfer. GaInSn also has a low specific heat of 1/14 of water,[13] allowing for a higher temperature change in a magnetic refrigerator. Studies show that the use of GaInSn can reduce the size of system components and costs, making it a promising choice for MR.[6,14] At lower operating frequencies, however, the manufacturing cost of using a GaInSn liquid metal is higher than that of a water−ethanol mixture. Nevertheless, as the frequency increases, the GaInSn liquid metal becomes a more cost-effective choice. For instance, at 2 Hz, a magnetic refrigerator based on the GaInSn liquid metal was 2.5 times less expensive than a system based on a water−ethanol mixture.[6,14]

In a study, researchers compared the performance of six different working fluids and two different geometries of the magnetocaloric material in a magnetic refrigerator.[6,15,16] They found that GaInSn liquid metal, despite its higher viscosity, outperformed water−alcohol-based mixtures in terms of specific cooling energy and maximum coefficient of performance, particularly at 2 Hz and in parallel plate geometry. This is due to the significantly higher thermal diffusivity of GaInSn liquid metal, which is 3 orders of magnitude higher than that of water−alcohol mixtures.

$La(Fe,Si)_{13}$ represents a promising magnetocaloric material owing to its low material cost, better adiabatic temperature change and isothermal entropy change, and the possibility to tune its Curie temperature depending on the applications.[17−20] Preparation of the $La(Fe,Si)_{13}$ alloy family with a single $NaZn_{13}$ phase is challenging.[21,22] Certain manufacturing processes require the addition of excess La, which is subsequently removed.[23,24] Depending on the degree of removal, it results in an alloy with insufficient or excess La, leading to, among others, the formation of the α-Fe phase.[25−28] It also affects the magnetic entropy change, either favorably or unfavorably.[29−32] Improvements are needed in the mechanical stability of the $La(Fe,Si)_{13}$ alloy family, which is the focus of several studies.[22,32−38]

The contact between the heat transfer fluid, such as water, water−alcohol mixture, or aqueous solutions, and the $La(Fe,Si)_{13}$ family, given its high Fe content, would result in corrosion.[39−44] Therefore, various studies have been focused on addressing this problem. For example, the exposure of $La(Fe,Co,Si)_{13}C_{0.15}$ to distilled water over a week resulted in a magnetic entropy change to decrease from 8.1 to 7.7 J kg^{-1} K^{-1} under a 0 to 3 T field change.[45] Studies involved immersing $La(Fe,Mn,Si)_{13}H_z$ particles in two kinds of media: deionized water and deionized water with corrosion inhibitors. It was found that the presence of a corrosion inhibitor is crucial to maintain the chemical stability of the magnetocaloric materials.[46] A magnetic field was also found to influence the chemical stability of $La(Fe, Si)_{13}$ alloys immersed in deionized water—the direction of the magnetic field played a critical role in the corrosion rate.[47] For example, the sample immersed in deionized water for 3 days with exposure to 1 T parallel and 1 T perpendicular magnetic fields experienced a 56 and 22% reduction in its corrosion rate when compared to the case with zero magnetic field.[47]

Most previous studies that involved liquid metals have been numerical and assumed no chemical reaction between the liquid metal and the magnetocaloric material,[6] but recent experimental work has shown that this may not be the case. The mixture of liquid metal and a magnetocaloric material is critical for the performance of magnetic refrigerators, and any changes in their properties over time could significantly impact the efficiency and effectiveness of the technology. Therefore, it is important to conduct experimental studies to better understand the long-term impact of GaInSn on magnetocaloric materials.

de Castro et al.'s work on the preparation of a liquid metal-based magnetocaloric mixture was a critical step in this field, and their findings were significant in understanding the initial properties of the mixture.[11] However, more recent research by ORNL[48] and Lu et al.[49] has shown that the long-term effects of mixing GaInSn liquid metal and magnetocaloric materials are not yet fully understood. ORNL's unexpected increase in system pressure and Lu et al.'s observed reduction in peak-specific isothermal magnetic entropy change demonstrate that there may be chemical reactions occurring between the GaInSn liquid metal and magnetocaloric materials that could impact the performance of magnetic refrigerators over time.

In this new study, we address this gap in understanding by investigating the effects of mixing Calorivac H ($La(Fe,Mn,Si)_{13}H_z$) with GaInSn alloy over an extended period of 85 weeks. By analyzing the specific isothermal magnetic entropy change and specific cooling energy over time, we aim to provide new insights into the long-term performance of liquid metal-based MR systems. Our findings could pave the way for more efficient and reliable MR technologies in the future.

2. METHODOLOGY

Gallium (99.99% purity), indium (99.995% purity), and tin (99.9% purity) purchased from Polymet, Germany, were taken at 68.5/21.5/10 wt %, respectively, and were melted in an electric heater. It was then cooled by natural convection and remained in the liquid state at room temperature. The $La(Fe,Mn,Si)_{13}H_z$ material (Calorivac H) used for the study was purchased from Vacuumschmelze GmbH, Germany, in powder form with a particle size of less than 250 μm. These particles were initially milled manually in a mortar and pestle for 20 min. This was followed by the mixture preparation, in which 20 wt % of $La(Fe,Mn,Si)_{13}H_z$ and GaInSn liquid metal was milled in a mortar and pestle for 20 min in air at room temperature. However, as discussed later, the particles were not homogeneously distributed. The resulting mixture, like the liquid metal, forms an oxide layer which is typical of GaInSn. The mixture from the mortar was transferred using a pipet dropper to a cylindrical sample holder (Quantum Design VSM sample holder—P125E). It had a diameter of 2 mm and a length of 4 mm. The top was sealed to avoid any leakage. The magnetization−temperature ($M-T$) measurements were taken in the Vibrating Sample Magnetometer option of the Physical Property Measurement System, Quantum Design Inc. For each $M-T$ measurement discussed in this report, the sample was

https://doi.org/10.1021/acsomega.3c06724
ACS Omega 2023, 8, 49027−49036

initially heated from room temperature to 350 K at zero magnetic field, which is nearly 60 K above the Curie temperature of the magnetocaloric material considered (291.5 K), and held there for 10 min. The differential scanning calorimetry (DSC) measurements were performed in NETZSCH DSC 214 Polyma.

3. RESULTS AND DISCUSSION

In the remainder of this article, MCM refers to La-(Fe,Mn,Si)$_{13}$H$_z$ (Calorivac H), while liquid metal refers to the GaInSn alloy. The mixture of Calorivac H with GaInSn liquid metal is simply referred to as the mixture. The magnetization−temperature (M−T) measurement for the MCM and for the mixture on the day of preparation (Day 0) is shown in Figure 1. It should be noted that although 20 wt % of MCM was used in the mixture preparation, it was not homogeneously distributed in the liquid metal. As a result of this, when a sample was taken for magnetization measurement, it had 25.4 wt % of the MCM in the liquid metal. This wt % in the sample was determined by noting that when only the liquid metal was measured, it had negligible magnetization. It was, therefore, assumed that all of the measured magnetization of the mixture on Day 0 was due to MCM alone. By comparison of the magnetization of the mixture with that of the MCM, the weight percentage was determined. The magnetization value of the mixture shown in Figure 1 is normalized for the mass of the MCM in the mixture and, therefore, shows similar values to that of the MCM.

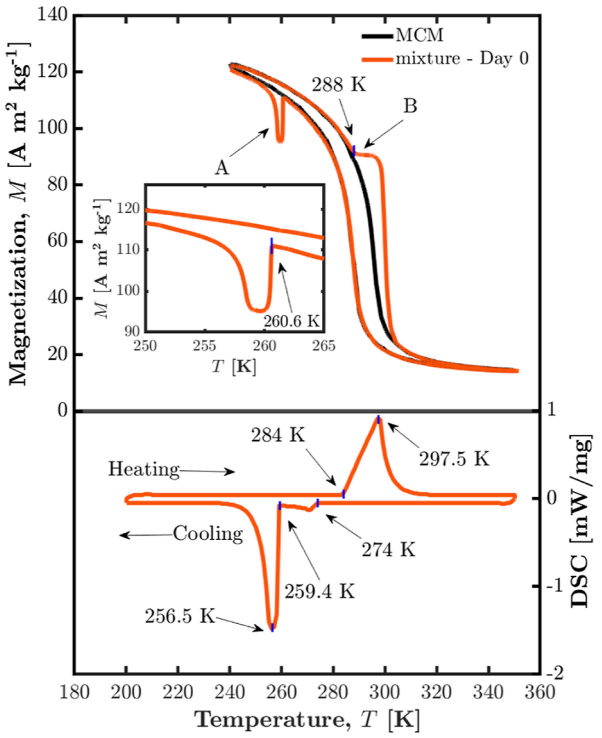

Figure 1. (Top) Magnetization−temperature measurements at $\mu_0 H$ = 1 T for the La(Fe,Mn,Si)$_{13}$H$_z$ (Calorivac H) particles and the mixture of GaInSn liquid metal with La(Fe,Mn,Si)$_{13}$H$_z$ (25.4 wt %) on the day of preparation (Day 0). The liquid metal had negligible magnetization. Therefore, the magnetization values of the mixture are normalized for the mass of the La(Fe,Mn,Si)$_{13}$H$_z$ in it. (Bottom) Zero-field DSC measurements of the mixture.

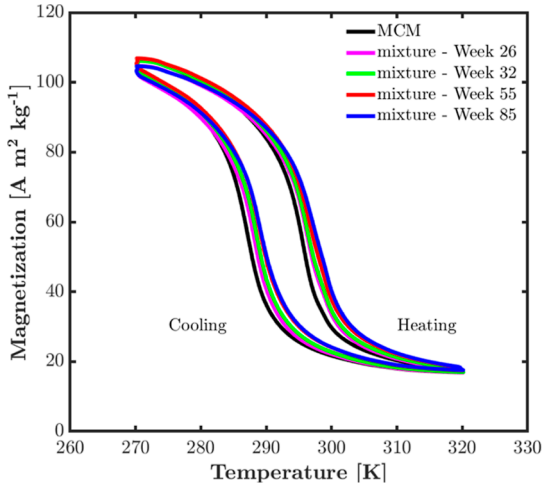

Figure 2. Magnetization−temperature (M−T) measurements at $\mu_0 H$ = 1 T for La(Fe,Mn,Si)$_{13}$H$_z$ particles and for the mixture of La(Fe,Mn,Si)$_{13}$H$_z$ (25.4 wt %) with GaInSn liquid metal are shown at different time periods. Since the GaInSn alloy remains in the liquid phase at 270 K, the magnetization behaviors observed in Figure 1 are not present here. The magnetization of the mixture appears to be higher than that of the MCM, but this is caused by an offset in the M−T curve of the mixture when compared to the MCM. There is a reduction in dM/dT for the mixture, as can be seen in Figure 3.

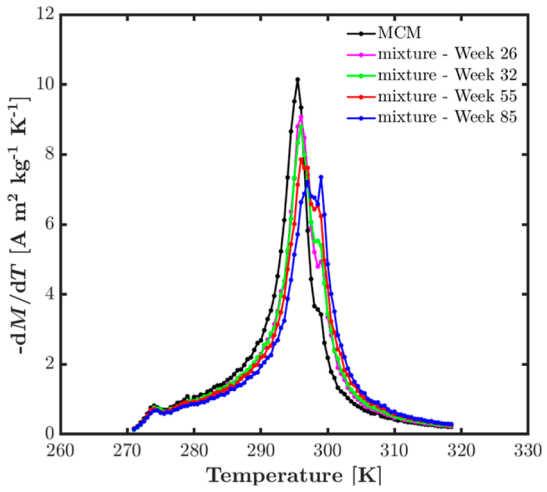

Figure 3. Plot of the derivative of magnetization with temperature for the heating curve is shown in Figure 2.

3.1. Effect of Phase Change of the Liquid Metal in the Mixture.

Even though the liquid metal has a negligible quantitative contribution to the magnetization of the mixture, its qualitative effect is noticeable. This can be seen by observing the two regions marked as A and B in Figure 1, where the M−T curve of the mixture deviates from that of the MCM. These are attributed to the phase change behavior of liquid metal between its liquid and solid states, as seen from the zero-field DSC results for the mixture at the bottom of Figure 1. For regions A and B, the minor differences in the onset temperature between the magnetometry and DSC data in Figure 1 are due to (i) the M−T measurements were taken at 1 T, while the DSC measurements were taken at zero-field; (ii) the temperature measured by the magnetometer is that of the sample chamber, while it is the sample holder for the DSC. Further, the small dip at 274 K in the DSC data is due to

https://doi.org/10.1021/acsomega.3c06724
ACS Omega 2023, 8, 49027−49036

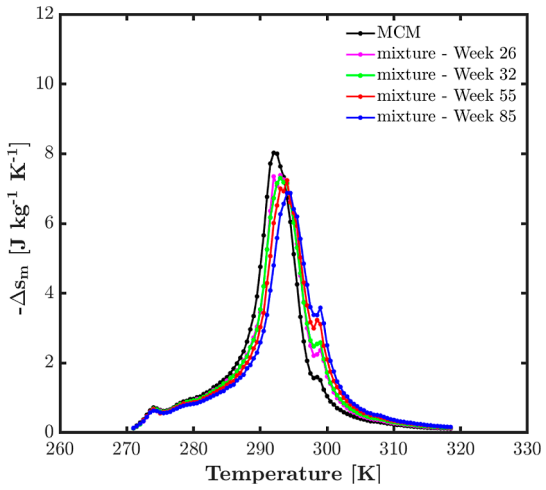

Figure 4. Plot of the specific isothermal magnetic entropy change (Δs_m) with temperature for the MCM and the mixture at $\mu_0\Delta H$ = 1 T. It can be seen that the primary peak decreases with time, while the secondary peak increases with time for the mixture when compared to that of the MCM.

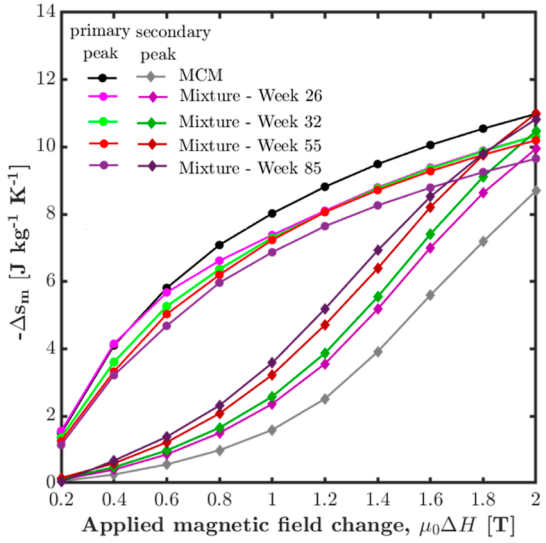

Figure 5. Plot of the primary and secondary peaks in the specific isothermal magnetic entropy change (Δs_m) for the $La(Fe,Mn,Si)_{13}H_z$ and the mixture of $La(Fe,Mn,Si)_{13}H_z$ with GaInSn liquid metal as a function of the change in the applied magnetic field.

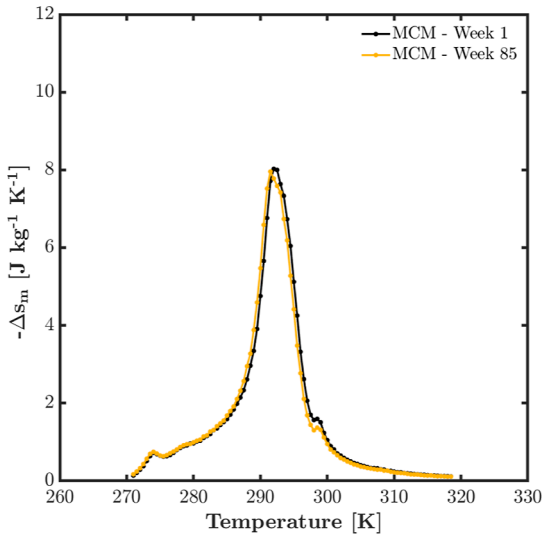

Figure 6. Plot of the specific isothermal magnetic entropy change (Δs_m) with temperature for the $La(Fe,Mn,Si)_{13}H_z$ on week 1 and 85 for $\mu_0\Delta H$ = 1 T. Over the 85 week period, the MCM was subjected to twice the number of $M-T$ measurements and thus Curie temperature transitions when compared with that of the mixture.

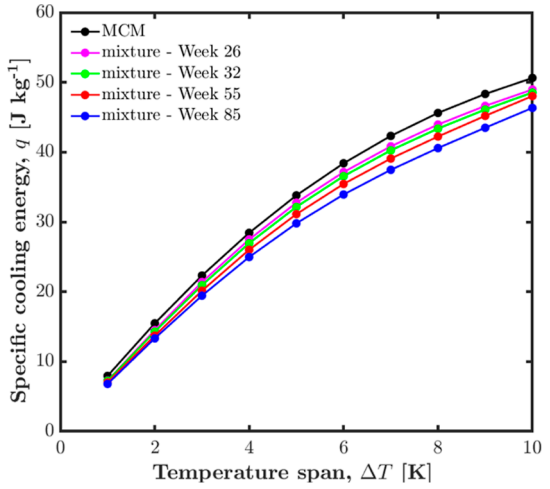

Figure 7. Specific cooling energy (eq 2) at $\mu_0\Delta H$ = 1 T as a function of temperature span centered around the Curie temperature (i.e., peak Δs_m value) for the MCM and the mixture. Geometrically, this value represents the area under the Δs_m-T curve shown in Figure 4 for the appropriate temperature span.

metastatic or peritectic reactions, in which the solidification of the metal phase occurs at different temperatures.[50]

The dip in magnetization observed during the cooling cycle (section A in Figure 1) is caused by the supercooling of the liquid metal and subsequent exothermic crystallization.[51,52] This is reflected as a sudden drop, followed by an almost steady value, and finally, a combination of steep and gradual increases in the magnetization.

The sudden drop is caused due to the heat released by the crystallization of the supercooled liquid metal, which passes from the liquid state at the supercooled temperature to the liquid state at the liquid−solid phase change temperature, which is at a relatively higher temperature. This is followed by a phase change of the liquid metal to the solid state. During this transition, the temperature and, thereby, the magnetization of the mixture are maintained at a nearly steady value. When the phase change is complete, the temperature of the liquid metal and the mixture decreases. During this process, the temperature of the space surrounding the sample in the magnetometer is at a much lower temperature. Since the time rate of heat transfer between the sample and its surroundings is proportional to their temperature difference, the drop in temperature and, therefore, the magnetization of the mixture are initially steep and are followed by a gradual reduction. In addition, the density changes in the liquid metal during crystallization can cause mechanical stress on the MCM particles in the mixture, which can also contribute to the observed reduction in the magnetization.

During heating, as the liquid metal in the mixture changes from the solid to the liquid phase, its temperature and, therefore, that of the mixture remain constant. Due to this, a constant magnetization is observed in section B in Figure 1.

https://doi.org/10.1021/acsomega.3c06724
ACS Omega 2023, 8, 49027−49036

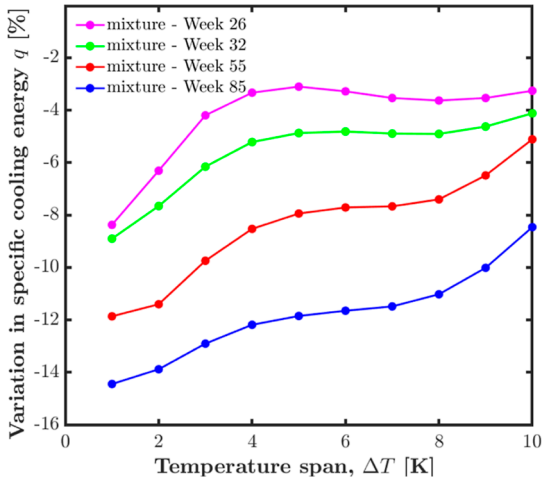

Figure 8. Reduction in specific cooling energy for the mixture when compared with the MCM for the data is shown in Figure 7. It is seen in general that the reduction is higher at lower temperature spans, and this decreases at higher temperature spans.

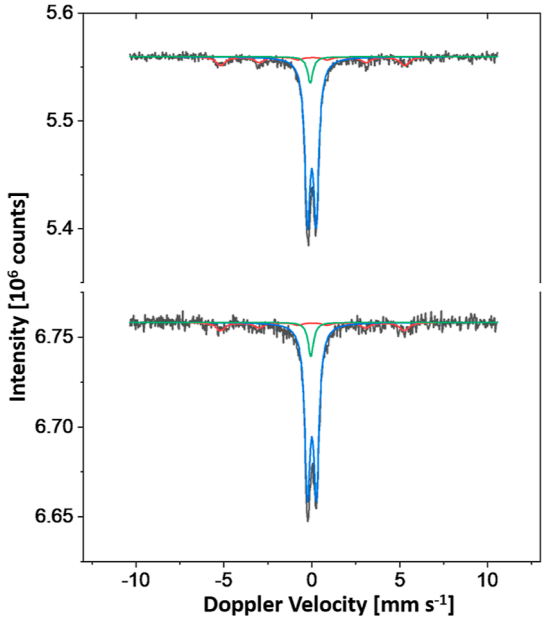

Figure 9. Mössbauer spectra at 300 K for the MCM (top) and the mixture (bottom). The red line indicates the α-Fe phase, while the green line indicates the Fe_I phase and the blue line indicates the Fe_{II} phase.

Note that the horizontal axis of Figure 1 shows the temperature of the space surrounding the sample, as measured by the magnetometer, and not the temperature of the sample itself. Generally, these deviate only slightly, but during a phase-transition releasing or consuming latent heat, the deviations may be significant.

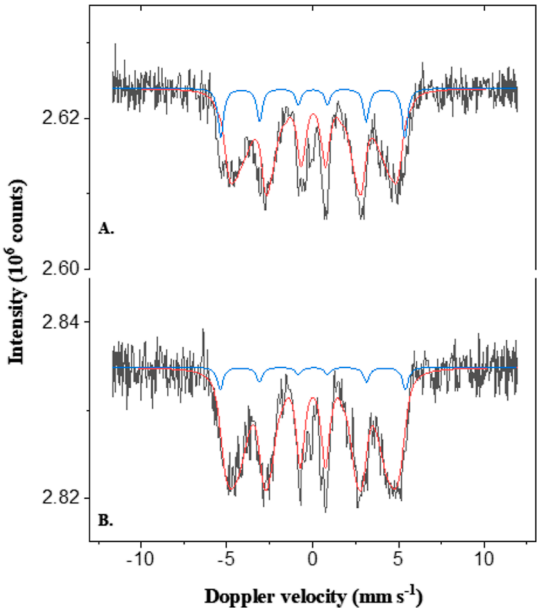

Figure 10. Mössbauer spectra at 120 K for the MCM (top) and the mixture (bottom). The blue line indicates the α-Fe phase, while the red line indicates the Fe_I + Fe_{II} phase.

3.2. Isothermal Magnetic Entropy Change. From the application point of view of MR, it is desirable to know the variation of the magnetocaloric effect of the mixture over the long-term, and here, we report it over a period of 1.5 years (85 weeks). For this purpose, the specific isothermal magnetic entropy change, Δs_m given by eq 1,[53] which is considered to be a parameter that quantifies the magnetocaloric effect, is determined for the mixture up to $\mu_0\Delta H$ = 2 T. This value was chosen because magnetocaloric refrigerators primarily use permanent magnets as magnetic field sources, as the use of electromagnets is not viable in terms of efficiency to compete with vapor compression refrigeration. As the magnetocaloric effect is proportional to $\mu_0\Delta H$, permanent magnets are designed to generate as high a field as possible. Depending on the design, these are typically in the range of 1−2 T, with 1 T being preferred due to its relative simplicity of construction and lower cost.

$$\Delta s_m(T,\Delta H) = \int_{H_i}^{H_f} \left(\frac{\partial M(T,H)}{\partial T}\right)_H dH \quad (1)$$

Table 1. Mössbauer Fitted Parameters for the Spectra Shown in Figure 9 Measured at 300 K[a]

Sample	Isomer shift (mm/s)	Electric quadrupole splitting (mm/s)	Hyperfine field (T)	Linewidth (mm/s)	Phase	Spectral contribution (%)
$La(Fe,Mn,Si)_{13}H_z$ (Calorivac H)	0.05(2)	N/A	32.5(1)	0.63(5)	α-Fe	16(3)
	0.00(1)	0.48(1)	N/A	0.36(1)	Fe_I	77(1)
	−0.09(2)	N/A	N/A	0.36(2)	Fe_{II}	7(3)
$La(Fe,Mn,Si)_{13}H_z$ + GaInSn	0.03(2)	N/A	32.5(1)	0.64(5)	α-Fe	14(3)
	0.00(1)	0.49(1)	N/A	0.37(1)	Fe_I	78(1)
	−0.06(2)	N/A	N/A	0.37(2)	Fe_{II}	8(3)

[a]The number in parentheses indicates the measurement uncertainty in the last digit.

https://doi.org/10.1021/acsomega.3c06724
ACS Omega 2023, 8, 49027−49036

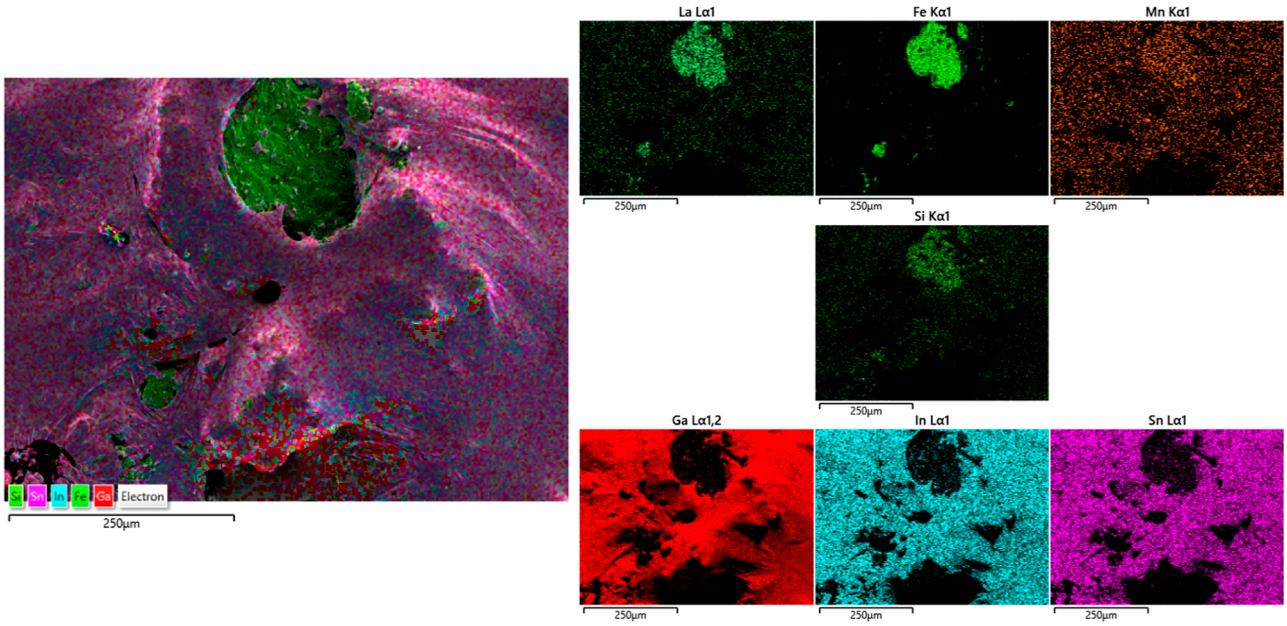

Figure 11. Scanning electron microscopy image of the mixture of Calorivac H particles in GaInSn liquid metal after 55 weeks. Energy dispersive spectroscopy shows the constituent elements—La, Fe, Mn, and Si for the MCM and Ga, In, and Sn for the liquid metal.

Table 2. Mössbauer Fitted Parameters for the Spectra Shown in Figure 9 Measured at 120 K[a]

Sample	Isomer shift (mm/s)	Electric quadrupole splitting (mm/s)	Hyperfine field (T)	Linewidth (mm/s)	Phase	Spectral contribution (%)
$La(Fe,Mn,Si)_{13}H_z$ (Calorivac H)	0.02(1)	N/A	33.4(1)	0.39(3)	α-Fe	14(3)
	0.04(1)	0.01(2)	26.9(1)	0.50(3)	Fe_I + Fe_{II}	86(3)
$La(Fe,Mn,Si)_{13}H_z$ + GaInSn	0.02(1)	N/A	33.5(1)	0.41(3)	α-Fe	6(3)
	0.01(1)	−0.01(2)	27.9(1)	0.50(3)	Fe_I + Fe_{II}	94(3)

[a]The number in parentheses indicates the measurement uncertainty in the last digit. For the Fe_I + Fe_{II} phase, the hyperfine field is the average magnetic field.

To calculate Δs_m, eq 1 is numerically integrated by measuring the variation in the magnetization of the mixture with temperature for the applied magnetic field from 0 to 2 T with a step size of 0.2 T. The temperature range of the measurement is chosen to be in the region of the Curie temperature (291.5 K), which would be the operating temperature of the mixture in a magnetic refrigerator. This is because the magnetocaloric effect is maximum when the change in magnetization with temperature is maximum, which is at the Curie temperature of the MCM, where a magnetic phase transition from the ferromagnetic to the paramagnetic phase occurs.

A temperature range of 270−320 K is therefore selected for further magnetization measurements. This is shown in Figure 2 for the mixture on weeks 26, 32, 55, and 85 and for the MCM at $\mu_0 H$ = 1 T. Note that in this temperature range, the liquid metal remains in the liquid state. Therefore, the implications of solidification and melting of the liquid metal observed in Figure 1 are not present in Figure 2. Also, in Figure 2, it appears that the magnetization of the mixture increases with time, and it is higher than that of the MCM, which is indeed not true. They appear this way because of the offset in the $M-T$ curve for the mixture. Furthermore, as noted above, the magnetocaloric effect is proportional to $(\partial M/\partial T)_H$, and the same for the mixture decreases with time when compared with that of the MCM, as shown in Figure 3.

The variation of Δs_m with temperature for the MCM and the mixture is shown in Figure 4 for $\mu_0 \Delta H$ = 1 T, calculated from the heating curves of the corresponding $M-T$ data. For each case in Figure 4, a primary peak is followed by a secondary peak at a higher temperature. Note that for the partially hydrogenated $La(Fe,Si)_{13}H_x$ material system, it is known that the sharp magnetic phase transition is unstable.[54−56] The possible reason could be the diffusion of the hydrogen atoms from the lower volume paramagnetic to the higher volume ferromagnetic phase since the ferromagnetic lattice volume is about 1−2% larger than the paramagnetic state volume for this iso-structural transition.[54] As a result, it will cause local variations in the hydrogen segregation and, hence, an inhomogeneous distribution of critical temperatures (i.e., the secondary peak). The possible segregated secondary phase can also be observed in the $M-T$ curve (Figure 2) and the dM/dT curve (Figure 3). It is worth mentioning that the phase segregation phenomenon can be suppressed by homogenization annealing.[55]

From Figure 4, a reduction in the peak Δs_m value with time for the mixture compared to the MCM is observed and is discussed next.

3.2.1. Reduction in Δs_m Values. For $\mu_0 \Delta H$ of 1 T (Figure 4), the peak Δs_m value is 8.0 J kg^{-1} K^{-1} for the MCM. For the mixture, the peak Δs_m value decreases to 7.4 (−7.5%), 7.3 (−8.7%), 7.2 (−10.0%), and 6.9 (−13.7%) J kg^{-1} K^{-1} at weeks 26, 32, 55, and 85, respectively. In each case, the secondary peak shows an opposite trend to the primary peak; i.e., the secondary peak increases with time for the mixture. The secondary peak Δs_m value is 1.6 J kg^{-1} K^{-1} for the MCM, while

https://doi.org/10.1021/acsomega.3c06724
ACS Omega 2023, 8, 49027−49036

it is 2.4 (+50.0%), 2.6 (+62.5%), 3.3 (+106.2%), and 3.6 (+125.0%) J kg^{-1} K^{-1} for the mixture at weeks 26, 32, 55, and 85, respectively. In the first 26 weeks, the primary peak Δs_m value decreases by 0.6 J kg^{-1} K^{-1} for the mixture, while in the last 30 weeks (between weeks 55 and 85), the decrease is only 0.3 J kg^{-1} K^{-1}. Thus, the primary peak Δs_m value for the mixture seems to settle at a 14% reduction level after 1.5 years compared to the MCM. Similarly, the increase in the secondary peak Δs_m value in the first 26 weeks is 0.8 J kg^{-1} K^{-1}, while in the last 30 weeks, it increases by 0.3 J kg^{-1} K^{-1}. So, the secondary peak seems to settle near a 125% increased level.

The variation in the primary and secondary peak Δs_m values for the mixture as a function of $\mu_0\Delta H$ is shown in Figure 5. It can be seen that for $\mu_0\Delta H < 1$ T, the reduction in the primary peak Δs_m value is gradual with time. For $\mu_0\Delta H > 1$ T, the primary peak Δs_m value seems to stabilize between weeks 26 and 55 before continuing to decrease between weeks 55 and 85. The trend of increase in the secondary peak Δs_m values of the mixture with time is relatively similar for different $\mu_0\Delta H$, while they coincide at 2 T. The slope of the change in Δs_m value with $\mu_0\Delta H$ is decreasing for the primary peak, while it is increasing for the secondary peak for $\mu_0\Delta H$ up to 1.6 T, after which it begins to decrease. Also, the secondary peak Δs_m value for the mixture is lower than its primary peak Δs_m value for $\mu_0\Delta H$ up to 1.6 T. The formation of such secondary peaks is well-known for the partially hydrogenated MCM family of materials, which is caused by hydrogen mobility between the magnetic phases present.[57,58] The MCM was subjected to twice the number of $M-T$ measurements, and thus Curie temperature transitions, over an 85 week period when compared with that of the mixture. However, in contrast to the mixture, its Δs_m profile remained relatively unchanged, as can be seen in Figure 6. While it is useful to know the changes in peak Δs_m values, the performance of the magnetocaloric mixture in the refrigerator depends on the distribution of Δs_m over a finite operating temperature range and will be discussed next.

3.2.2. Cooling Power. When the MCM is utilized for refrigeration, it is important to know the amount of heat that it can transport per unit mass from the low-temperature side (T_L) to the high-temperature side (T_H). This is determined by the specific cooling energy (q) and is characterized by the variation of the specific isothermal magnetic entropy change in the temperature range of interest, as given by eq 2:[53]

$$q = -\int_{T_L}^{T_H} \Delta s_m(T)_{\Delta H}\, dT \quad (2)$$

The temperature span required for typical refrigeration applications is in the range of 10−40 K. However, the maximum adiabatic temperature change (another measure of magnetocaloric effect) for typical magnetocaloric materials is less than ≈6 K for $\mu_0\Delta H$ = 2 T. Furthermore, the MCM considered is of the first-order magnetic transition type, which exhibits a relatively narrow temperature range (for example, 5 to 10 K) of useful magnetocaloric effect when compared with the second-order magnetic transition materials such as Gd. However, unlike Gd, materials such as $La(Fe,Mn,Si)_{13}H_z$, and MnFePSi, which though they have hysteresis issues, are relatively less costly, made from widely available materials, and their Curie temperature can be tuned by altering their composition while still retaining a significant magnetocaloric effect.

To extend the operating temperature range of magnetic refrigerators, layered materials are typically used in so-called active magnetic regenerators, where the Curie temperatures of adjacent layers vary progressively. For systems based on the magnetocaloric mixture discussed in Section 1, a cascade arrangement of loops can be used with the Curie temperature of adjacent loops varying progressively. In either case, each material undergoes its own thermodynamic cycle. Thus, the temperature range of interest in eq 2 is in the range of 5−10 K.

The variation in the specific cooling energy as a function of the temperature span is plotted in Figure 7 for the MCM and the mixture. The % variation of q for the mixture as compared to the MCM is plotted in Figure 8. It can be seen that q continues to decrease up to the investigated period of 85 weeks. For example, over a temperature span of interest, i.e., 5 K, the reduction in q is 3, 4, 8, and 12% on weeks 26, 32, 55, and 85, respectively. This indicates that the specific cooling energy has decreased over a period of 1.5 years and may continue to do so. The reduction in specific cooling energy decreases significantly over a temperature span of 9−12 K (Figure 7). This is caused by the inclusion of a secondary peak in Δs_m-T (Figure 4) in the specific cooling energy calculation as the temperature span increases (eq 2). The reduction in q is greater at lower temperature spans and continues to decrease as the temperature span increases. Analysis over a broader span of 40 K shows that the reduction in q is less than l%. This indicates that although Δs_m has decreased near the Curie temperature of the magnetocaloric material, the increase in other temperatures is such that the area under the Δs_m-T curve, as measured by q over a span of 40 K, has remained essentially unchanged. However, for applications in MR, the reduction in q over a 5 K temperature span is of importance. To ascertain for any changes in the material, Mössbauer spectroscopy measurement is carried out, as Fe is the major component in the MCM and is discussed next.

3.2.3. Mössbauer Spectroscopy. Transmission ^{57}Fe Mössbauer spectra were collected at 300 K with a conventional constant-acceleration spectrometer using a ^{57}Co(Rh) source. Velocity calibration was carried out using α-Fe foil at room temperature. The Mössbauer spectra were fitted using the Mosswinn 4.0 program.[59]

Mössbauer measurements were performed at 300 K ($>T_c$ = 291.5 K) for the MCM, and the mixture is presented in Figure 9, and the fitted parameters are shown in Table 1. A predominantly doublet profile is observed in the spectra. Note that the MCM material belongs to the $NaZn_{13}$ crystal structure and has two nonequivalent Fe sites—Fe_I(8b) and Fe_{II}(96i). Of these, the former results in a relatively low magnitude singlet, and the latter results in a relatively high magnitude doublet, as observed in materials with similar composition.[60] Furthermore, the α-Fe phase is observed for the present material, as also reported in[61] for a material with a similar composition.

The isomer shift, quadrupole split, and hyperfine fields for the mixture (Table 1) show almost no change compared with the MCM (taking into account the measurement uncertainty). From this, we infer that the chemical environment of Fe is not altered. Thus, the observed decrease in Δs_m near the Curie temperature could be caused by the formation of two peaks attributed to the unstable nature of H. However, even when the unmixed MCM was subjected to twice as many (de)magnetization cycles as the mixture, no such phase segregation of hydrogen was observed (Figure 6). Therefore,

https://doi.org/10.1021/acsomega.3c06724
ACS Omega 2023, 8, 49027−49036

the reason for its formation in the mixture requires further analysis.

For the observed reduction of q in the mixture, apart from measurement uncertainty, one possibility could be due to a weak chemical reaction between other elements in the MCM and the liquid metal. For example, in a study on the alloying behavior between magnetocaloric MnFeNiGeSi and GaInSn by Lu et al.,[49] they identified the formation of a scarce Mn−Ga alloy that is not magnetocaloric. They also reported no chemical reaction between Fe and GaInSn. Therefore, for the present mixture, such a formation of Mn−Ga could be a possibility. A scanning electron microscopy image of the mixture with its oxide layer removed, taken after 55 weeks, is shown in Figure 11, along with the elemental maps. From this figure, it is seen that the elemental distributions of La, Fe, and Si are similar when compared to one another. Unlike this, Mn is relatively widespread, indicating the possibility of a Mn−Ga alloy formation.

Further, Mössbauer measurements for the MCM and the mixture were performed at 120 K, well below the Curie temperature ($>T_c$ = 291.5 K), as presented in Figure 10, and the fitted parameters are shown in Table 2. All the parameters remain nearly unchanged except the hyperfine field for Fe_I and Fe_{II}. The average hyperfine field for the Fe_I + Fe_{II} phase is higher for the mixture (27.9 T) when compared with the MCM (26.9 T). This is attributed to the formation of Mn−Ga alloy, which implies a reduction in the Mn content in the magnetocaloric material that is present in the mixture. Since Mn acts as a diluent in the magnetization measurement, its decreased content results in an increased hyperfine field for the mixture, which is in agreement with the literature.[62]

4. CONCLUSIONS

The use of a mixture of magnetocaloric material in liquid metal as a heat transfer fluid has been investigated for its potential application in magnetocaloric refrigerators. The magnetocaloric material $La(Fe,Mn,Si)_{13}H_z$ (Calorivac H) was selected due to its favorable magnetocaloric properties and suitability for commercial use. The nontoxic and nonflammable liquid metal GaInSn was chosen for its desirable characteristics. The report analyzed the impact of the GaInSn liquid metal on the magnetocaloric effect of $La(Fe,Mn,Si)_{13}H_z$ over a period of 1.5 years. The results of this study showed that the peak Δs_m value of the mixture decreased by approximately 14% when subjected to a magnetic field change of 1 T. Furthermore, the specific cooling energy (q) for a temperature span of 5 K decreased by 3 to 12% over a period of 26 to 85 weeks, respectively. Mössbauer spectroscopy analysis revealed that there were no significant changes in the chemical environment of Fe in the MCM. This indicates that the primary reason for the observed reduction in the magnetocaloric properties could be due to the formation of dual Δs_m peaks in the mixture caused by hydrogen mobility. A secondary reason could be due to the alloying behavior between other elements in the MCM and the liquid metal.

In conclusion, the study suggests that utilizing a mixture of magnetocaloric material in liquid metal is a promising approach for developing highly efficient magnetocaloric refrigeration systems.

AUTHOR INFORMATION

Corresponding Author

Keerthivasan Rajamani − *Department of Thermal and Fluid Engineering, Faculty of Engineering Technology, University of Twente, 7500 AE Enschede, The Netherlands;* orcid.org/0000-0002-9311-2970; Email: k.rajamani@utwente.nl

Authors

Muhammet Sadaka Toprak − *Department of Applied Physics, KTH Royal Institute of Technology, SE 10691 Stockholm, Sweden;* orcid.org/0000-0001-5678-5298

Fengqi Zhang − *Fundamental Aspects of Materials and Energy, Faculty of Applied Sciences, Delft University of Technology, 2629 JB Delft, The Netherlands*

Achim Iulian Dugulan − *Fundamental Aspects of Materials and Energy, Faculty of Applied Sciences, Delft University of Technology, 2629 JB Delft, The Netherlands*

Ekkes Brück − *Fundamental Aspects of Materials and Energy, Faculty of Applied Sciences, Delft University of Technology, 2629 JB Delft, The Netherlands*

Theo van der Meer − *Department of Thermal and Fluid Engineering, Faculty of Engineering Technology, University of Twente, 7500 AE Enschede, The Netherlands*

Mina Shahi − *Department of Thermal and Fluid Engineering, Faculty of Engineering Technology, University of Twente, 7500 AE Enschede, The Netherlands*

Complete contact information is available at: https://pubs.acs.org/10.1021/acsomega.3c06724

Notes

The authors declare no competing financial interest.

ACKNOWLEDGMENTS

The authors would like to thank the Netherlands Organization for Scientific Research (NWO) for (partially) financing the present work, which is part of the research program NETMNF with project number 15401.

REFERENCES

(1) Gschneidner, K., Jr; Pecharsky, V.; Pecharsky, V. Thirty years of near room temperature magnetic cooling: Where we are today and future prospects. *Int. J. Refrig.* **2008**, *31* (6), 945−961.

(2) Agency, I. E. *The Future of Cooling: Opportunities for energy-efficient air conditioning*; OECD Publishing, 2018.

(3) Franco, V.; Blázquez, J.; Ingale, B.; Conde, A. The magnetocaloric effect and magnetic refrigeration near room temperature: materials and models. *Annu. Rev. Mater. Res.* **2012**, *42*, 305−342.

(4) Brück, E. Chapter four magnetocaloric refrigeration at ambient temperature. *Handb. Magn. Mater.* **2007**, *17*, 235−291.

(5) Porcari, G.; Morrison, K.; Cugini, F.; Turcaud, J.; Guillou, F.; Berenov, A.; Van Dijk, N.; Brück, E.; Cohen, L.; Solzi, M. Influence of thermal conductivity on the dynamic response of magnetocaloric materials. *Int. J. Refrig.* **2015**, *59*, 29−36.

(6) Kitanovski, A.; Tušek, J.; Tomc, U.; Plaznik, U.; Ožbolt, M.; Poredoš, A. *Magnetocaloric energy conversion*; Springer, 2016.

(7) Egolf, P. W.; Gendre, F.; Kitanovski, A.; Sari, O. *Machbarkeitsstudie für magnetische wärmepumpen: Anwendungen in der schweiz - schlussbericht, Swiss Federal Office of Energy*, Research unit - SFOE, Project number: 100873(Table 20); SFOE, 2006.

(8) Mason, P. E.; Uhlig, F.; Vaněk, V.; Buttersack, T.; Bauerecker, S.; Jungwirth, P. Coulomb explosion during the early stages of the reaction of alkali metals with water. *Nat. Chem.* **2015**, *7* (3), 250−254.

(9) Liu, T.; Sen, P.; Kim, C.-J. Characterization of nontoxic liquid-metal alloy galinstan for applications in microdevices. *J. Microelectromech. Syst.* **2012**, *21* (2), 443−450.

https://doi.org/10.1021/acsomega.3c06724
ACS Omega 2023, 8, 49027−49036

(10) Li, G.; Wu, X.; Lee, D.-W. A galinstan-based inkjet printing system for highly stretchable electronics with self-healing capability. *Lab Chip* **2016**, *16* (8), 1366−1373.
(11) de Castro, I. A.; Chrimes, A. F.; Zavabeti, A.; Berean, K. J.; Carey, B. J.; Zhuang, J.; Du, Y.; Dou, S. X.; Suzuki, K.; Shanks, R. A.; et al. A gallium-based magnetocaloric liquid metal ferrofluid. *Nano Lett.* **2017**, *17* (12), 7831−7838.
(12) Yang, T.; Kwon, B.; Weisensee, P. B.; Kang, J. G.; Li, X.; Braun, P.; Miljkovic, N.; King, W. P. Millimeter-scale liquid metal droplet thermal switch. *Applied Physics Letters* **2018**, *112* (6), DOI: 10.1063/1.5013623.
(13) Hodes, M.; Zhang, R.; Lam, L. S.; Wilcoxon, R.; Lower, N. On the potential of galinstan-based minichannel and minigap cooling. *IEEE Trans. Compon., Packag., Manuf. Technol.* **2014**, *4* (1), 46−56.
(14) Egolf, P. W.; Kitanovski, A.; Gonin, C. *Central magnetic cooling and refrigeration machines (chiller) and their assessment a feasibility study*, Research unit - SFOE, Contract number - 102873, Project number: 153691(Table 20); SFOE, 2010.
(15) Tušek, J.; Kitanovski, A.; Prebil, I.; Poredoš, A. Dynamic operation of an active magnetic regenerator (AMR): Numerical optimization of a packed-bed AMR. *Int. J. Refrig.* **2011**, *34* (6), 1507−1517.
(16) Tušek, J.; Kitanovski, A.; Poredoš, A. Geometrical optimization of packed-bed and parallel-plate active magnetic regenerators. *Int. J. Refrig.* **2013**, *36* (5), 1456−1464.
(17) Zarkevich, N. A.; Zverev, V. I. Viable materials with a giant magnetocaloric effect. *Crystals* **2020**, *10* (9), 815.
(18) Kamran, M. S.; Ahmad, H. O.; Wang, H. S. Review on the developments of active magnetic regenerator refrigerators−evaluated by performance. *Renewable Sustainable Energy Rev.* **2020**, *133*, 110247.
(19) Gottschall, T.; Skokov, K. P.; Fries, M.; Taubel, A.; Radulov, I.; Scheibel, F.; Benke, D.; Riegg, S.; Gutfleisch, O. Making a cool choice: the materials library of magnetic refrigeration. *Adv. Energy Mater.* **2019**, *9* (34), 1901322.
(20) Lionte, S.; Barcza, A.; Risser, M.; Muller, C.; Katter, M. LaFeSi-based magnetocaloric material analysis: Cyclic endurance and thermal performance results. *Int. J. Refrig.* **2021**, *124*, 43−51.
(21) Fujieda, S.; Fukamichi, K.; Suzuki, S. Microstructure and isothermal magnetic entropy change of La (Fe0. 89 Si0. 11)13 in a single-phase formation process by annealing. *J. Alloys Compd.* **2013**, *566*, 196−200.
(22) Liu, J.; Moore, J.; Skokov, K.; Krautz, M.; Löwe, K.; Barcza, A.; Katter, M.; Gutfleisch, O. Exploring La (Fe, Si)13-based magnetic refrigerants towards application. *Scr. Mater.* **2012**, *67* (6), 584−589.
(23) Lu, X.; Zhang, Y.; Wang, F.; Zhang, M.; Liu, J. On the microstructural evolution and accelerated magnetocaloric phase formation in La-Fe-Si alloys by hot forging deformation. *Acta Mater.* **2021**, *221*, 117334.
(24) Sun, Y.; Lv, W.; Liang, Y.; Gao, Y.; Cui, W.; Yan, Y.; Zhao, W.; Zhang, Q.; Sang, X. Magnetocaloric properties of transition metal doped high entropy LaFe11Si2 alloys on Fe sites. *Scr. Mater.* **2023**, *223*, 115068.
(25) Hu, J.; Dong, Z.; Shen, Y.; Fu, B.; Zhang, B. Effect of excess lanthanum on corrosion and magnetocaloric property of LaFe11. 5 Si1. 5 compounds. *J. Rare Earths* **2019**, *37* (10), 1116−1120.
(26) Gębara, P.; Cesnek, M.; Bednarcik, J. Anomalous behavior of thermal expansion of α-fe impurities in the La (Fe, Co, Si)13-based alloys modified by Mn or selected lanthanides (Ce, Pr, Ho). *Curr. Appl. Phys.* **2019**, *19* (2), 188−192.
(27) Zhang, H.; Zhang, X.; Tan, J.; Yan, J.; Shi, H.; Zhang, J.; Wei, H.; Li, H.; Li, W.; Xia, A. Enhanced magnetocaloric properties and reduced annealing time of off-stoichiometric La1. 2Fe11. 6Si1. 4B0. 75 melt-spun ribbons. *J. Alloys Compd.* **2023**, *953*, 170114.
(28) Xian, L.; Yu, J.; Lin, W.; Ke, S.; Liu, C.; Nie, X.; Zhu, W.; Wei, P.; He, D.; Zhao, W.; et al. Preparation and magnetocaloric performance of La (Fe, Co, Si)13 alloys with wide transition temperature range. *Intermetallics* **2023**, *154*, 107827.
(29) Huang, X.; Dong, X.; Zhong, X.; Yao, S.; Huang, J.-H.; Liu, C.; Liu, J.; Liu, Z.; Ramanujan, R. Rapid formation of the magnetocaloric phase in La-Fe-Co-Si magnetocaloric alloys for near room temperature applications. *Intermetallics* **2023**, *157*, 107870.
(30) Wang, G.; Tan, X.; Yang, B.; Jing, T.; Zhao, Z.; Zhang, X. Hydrogenation and magnetocaloric effect in La-excessive La Fe11.5Si1.5 H alloys. *J. Alloys Compd.* **2020**, *816*, 152614.
(31) Lu, X.; Miao, L.; Zhang, Y.; Wang, Z.; Zhang, H.; Li, G.; Liu, J. First-order phase transition la-fe-si bulk materials with small hysteresis by laser powder bed fusion: Microstructure and magnetocaloric effect. *Scr. Mater.* **2023**, *232*, 115479.
(32) Li, G.; Zhong, X.; Huang, X.; Liu, C.; Huang, J.; Long, K.; Yu, H.; Liu, Z.; Ramanujan, R. Microstructure, magnetocaloric and mechanical properties of LaFe11. 8Si1. 2/Y64Co36 composites prepared by hot pressing and diffusion annealing. *J. Mater. Res.* **2023**, *38* (15), 3720−3729.
(33) Lyubina, J.; Schäfer, R.; Martin, N.; Schultz, L.; Gutfleisch, O. Novel design of La (Fe, Si)13 alloys towards high magnetic refrigeration performance. *Adv. Mater.* **2010**, *22* (33), 3735−3739.
(34) Law, J. Y.; Moreno-Ramírez, L. M.; Díaz-García, Á.; Franco, V. Current perspective in magnetocaloric materials research. *J. Appl. Phys.* **2023**, *133* (4), 040903.
(35) Waske, A.; Gruner, M. E.; Gottschall, T.; Gutfleisch, O. Magnetocaloric materials for refrigeration near room temperature. *MRS Bull.* **2018**, *43* (4), 269−273.
(36) Shao, Y.; Miao, X.; Zhang, Y.; Xu, F.; Liu, J. An in-depth review of La-Fe-Si magnetocaloric composites: Structure design and performance enhancement. *J. Magn. Magn. Mater.* **2022**, *564*, 170057.
(37) Miao, L.; Lu, X.; Wei, Z.; Zhang, Y.; Zhang, Y.; Liu, J. Enhanced mechanical strength in hot-rolled La-Fe-Si/Fe magnetocaloric composites by microstructure manipulation. *Acta Mater.* **2023**, *245*, 118635.
(38) Shao, Y.; Liu, J.; Zhang, M.; Yan, A.; Skokov, K. P.; Karpenkov, D. Y.; Gutfleisch, O. High-performance solid-state cooling materials: Balancing magnetocaloric and non-magnetic properties in dual phase La-Fe-Si. *Acta Mater.* **2017**, *125*, 506−512.
(39) Rocabert, U.; Muench, F.; Fries, M.; Beckmann, B.; Loewe, K.; Vieyra, H. A.; Katter, M.; Barcza, A.; Ensinger, W.; Gutfleisch, O. Electrochemical corrosion study of La (Fe11, 6-xSix1, 4Mnx) H1, 5 in diverse chemical environments. *Electrochim. Acta* **2022**, *434*, 141200.
(40) Sun, N.; Zhao, X.; Song, Y.; Liu, R.; Guo, J.; Zhang, Y.; Huang, J.; Zhang, Z. Electroless plating Ni-P coatings on La (Fe, Si)13 hydride bulks for room-temperature magnetic-refrigeration application. *J. Magn. Magn. Mater.* **2021**, *525*, 167685.
(41) Wojcieszak, S.; Wodajo, B.; Duong, A.; Hadimani, R. L.; Barua, R. A brief review on the chemical stability and corrosivity of magnetocaloric materials. *JOM* **2022**, *74* (11), 4368−4378.
(42) Xue, J.; Long, Y.; Wang, Y.; Zhou, H.; Zhang, H.; Ye, R. Corrosion behavior of nonstoichiometric La (Fe, Si)13-based alloys. *J. Phys. Chem. C* **2019**, *123* (47), 28898−28906.
(43) Guo, J.; Li, J.; Ye, R.; Wei, C.; Long, Y. Researches on corrosion behavior and magnetocaloric effect of the LaFe11. 7-xCoxAl1. 3 alloys. *J. Alloys Compd.* **2020**, *846*, 156298.
(44) Zhao, Q.; Yan, K.; Cui, Z.; Wen, B.; Xue, F.; Li, J.; Guo, J.; Xu, A.; Qiao, K.; Ye, R.; et al. Data driven accelerated design of high-efficiency corrosion inhibitor for magnetic refrigeration materials. *Corros. Sci.* **2023**, *216*, 111115.
(45) Hu, J.; Zhang, X.; Liu, H.; Fu, B.; Dong, Z.; Wang, Y. Microstructure, corrosion resistance, and magnetic properties of LaFe12. 35-x Co0. 65Si x C0. 15 (x= 1.3, 1.4, 1.5) compounds after corrosion in distilled water. *J. Supercond. Novel Magn.* **2022**, *35* (6), 1569−1574.
(46) Augusto Rosa, M.; Boeck, P.; Marciel Döring, A.; Peressoni Vieira, B.; Schafer, D.; Campos Plá Cid, C.; Andrés Lozano, J.; Riso Barbosa, J., Jr; Antônio Pereira Wendhausen, P.; da Silva Teixeira, C. Magnetocaloric La (Fe, Mn, Si)13Hz particles and their chemical stability in heat transfer fluids employed in magnetic refrigeration. *J. Magn. Magn. Mater.* **2022**, *563*, 169875.
(47) Zhu, C.; Miao, L.; Xie, J.; Xu, H.; Han, Y.; Liu, J.; Ryan, M. P.; Guo, L. Magnetic field effects on the corrosion behavior of

https://doi.org/10.1021/acsomega.3c06724
ACS Omega 2023, 8, 49027−49036

magnetocaloric alloys LaFe13. 9Si1. 4 under paramagnetic states. *J. Alloys Compd.* **2023**, *968*, 171901.
(48) Abuheiba, A. G.; Momen, A. M.; Zhang, M.; Rendall, J. D.; Barcza, A.; Vieyra, H. *Tech. rep.*; Oak Ridge National Lab.(ORNL): Oak Ridge, TN (United States), 2020.Benefit FOA FY2015-solid state magnetocaloric air conditioner
(49) Lu, Y.; Zhou, H.; Mao, H.; Tang, S.; Sheng, L.; Zhang, H.; Liu, J. Liquid metal-based magnetorheological fluid with a large magnetocaloric effect. *ACS Appl. Mater. Interfaces* **2020**, *12* (43), 48748−48755.
(50) Handschuh-Wang, S.; Gan, T.; Rauf, M.; Yang, W.; Stadler, F. J.; Zhou, X. The subtle difference between galinstan (r) and eutectic gainsn. *Materialia* **2022**, *26*, 101642.
(51) Handschuh-Wang, S.; Stadler, F. J.; Zhou, X. Critical review on the physical properties of gallium-based liquid metals and selected pathways for their alteration. *J. Phys. Chem. C* **2021**, *125* (37), 20113−20142.
(52) Koh, A.; Hwang, W.; Y Zavalij, P.; Chun, S.; Slipher, G.; Mrozek, R. Solidification and melting phase change behavior of eutectic gallium-indium-tin. *Materialia* **2019**, *8*, 100512.
(53) Gschneidner, K. A.; Pecharsky, V. K. Magnetocaloric materials. *Annu. Rev. Mater. Sci.* **2000**, *30* (1), 387−429.
(54) Baumfeld, O. L.; Gercsi, Z.; Krautz, M.; Gutfleisch, O.; Sandeman, K. G. The dynamics of spontaneous hydrogen segregation in LaFe13- xSixHy. *J. Appl. Phys.* **2014**, *115* (20), 203905.
(55) Fujita, A. Influence of electronic and metallographic structures on hydrogen redistribution in La(Fe, Si)13-based magnetocaloric compounds. *Acta Mater.* **2019**, *169*, 162−171.
(56) Zimm, C. B.; Jacobs, S. A. Age splitting of the La(Fe1-xSix)13Hy first order magnetocaloric transition and its thermal restoration. *J. Appl. Phys.* **2013**, *113* (17), 17A908.
(57) Barcza, A.; Katter, M.; Zellmann, V.; Russek, S.; Jacobs, S.; Zimm, C. Stability and magnetocaloric properties of sintered La(Fe, Mn, Si)$_{13}$H$_z$ alloys. *IEEE Trans. Magn.* **2011**, *47* (10), 3391−3394.
(58) Krautz, M.; Moore, J. D.; Skokov, K. P.; Liu, J.; Teixeira, C. S.; Schäfer, R.; Schultz, L.; Gutfleisch, O. Reversible solid-state hydrogen-pump driven by magnetostructural transformation in the prototype system La(Fe, Si)13Hy. *J. Appl. Phys.* **2012**, *112* (8), 083918.
(59) Klencsar, Z. Mössbauer spectrum analysis by evolution algorithm. *Nucl. Instrum. Methods Phys. Res., Sect. B* **1997**, *129* (4), 527−533.
(60) Wang, G.-j.; Wang, F.; Di, N.-l.; Shen, B.-g.; Cheng, Z.-h. Hyperfine interactions and band structures of LaFe13- xSix intermetallic compounds with large magnetic entropy changes. *J. Magn. Magn. Mater.* **2006**, *303* (1), 84−91.
(61) Makarov, S. I.; Krautz, M.; Salamon, S.; Skokov, K.; Teixeira, C. S.; Gutfleisch, O.; Wende, H.; Keune, W. Local electronic and magnetic properties of pure and Mn-containing magnetocaloric LaFe$_{13-x}$Si$_x$compounds inferred from Mössbauer spectroscopy and magnetometry. *J. Phys. D: Appl. Phys.* **2015**, *48* (30), 305006.
(62) Moreno-Ramírez, L. M.; Law, J. Y.; Borrego, J. M.; Barcza, A.; Greneche, J.-M.; Franco, V. First-order phase transition in high-performance La(Fe, Mn, Si)13H despite negligible hysteresis. *J. Alloys Compd.* **2023**, *950*, 169883.

https://doi.org/10.1021/acsomega.3c06724
ACS Omega 2023, 8, 49027−49036